1-1-2016

One-Pot Synthesis of Biocompatible Silver Nanoparticle Composites from Cellulose and Keratin: Characterization and Antimicrobial Activity

Chieu D. Tran
Marquette University, chieu.tran@marquette.edu

Franja Prosenc
University of Nova Gorica

Mladen Franko
University of Nova Gorica

Gerald Benzi
Marquette University

Accepted version. *ACS Applied Materials & Interfaces,* Vol. 8, No. 50 (2016): 34791-34801. DOI.

One-Pot Synthesis of Biocompatible Silver Nanoparticle Composites from Cellulose and Keratin: Characterization and Antimicrobial Activity

Chieu D. Tran
Department of Chemistry, Marquette University, Milwaukee, WI
Franja Prosenc
Laboratory for Environmental Research, University of Nova Gorica, Nova Gorica, Slovenia
Mladen Franko
Laboratory for Environmental Research, University of Nova Gorica, Nova Gorica, Slovenia
Gerald Benzi
Department of Chemistry, Marquette University, Milwaukee, WI

ACS Applied materials & Interfaces, Vol 8, No. 50 (2016): pg. 34791-34801. DOI.

Abstract

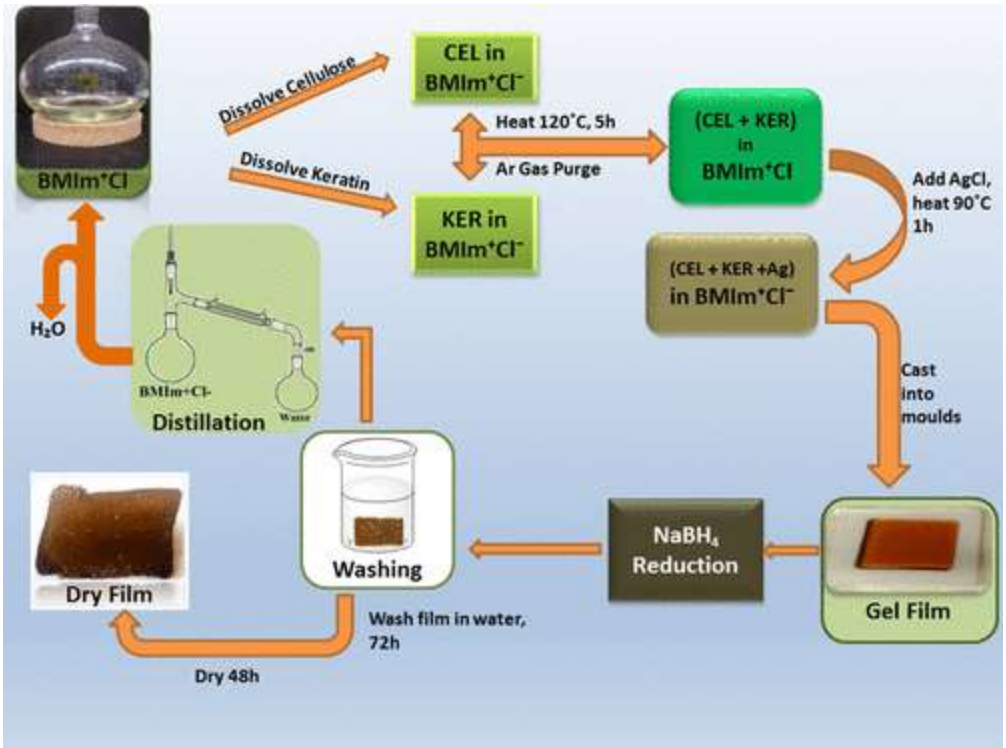

A novel, simple method was developed to synthesize biocompatible composites containing 50% cellulose (CEL) and 50% keratin (KER) and silver in the form of either ionic (Ag^+) or Ag^0 nanoparticles (Ag^+NPs or Ag^0NPs). In this method, butylmethylimmidazolium chloride ([$BMIm^+Cl^-$]), a simple ionic liquid, was used as the sole solvent and silver chloride was added to the [$BMIm^+Cl^-$] solution of [CEL+KER] during the dissolution process. The silver in the composites can be maintained as ionic silver (Ag^+) or completely converted to metallic silver (Ag^0) by reducing it with $NaBH_4$. The results of spectroscopy [Fourier transform infrared and X-ray diffraction (XRD)] and imaging [scanning electron microscopy (SEM)] measurements confirm that CEL and KER remain chemically intact and homogeneously distributed in the composites. Powder XRD and SEM results show that the silver in the [CEL+KER+Ag^+] and [CEL+KER+Ag^0] composites is homogeneously distributed throughout the composites in either Ag^+ (in the form of AgClNPs) or Ag^0NPs form with sizes of 27 ± 2 or 9 ± 1 nm, respectively. Both composites were found to exhibit excellent antibacterial activity against many bacteria including *Escherichia coli*, *Staphylococcus aureus*, *Pseudomonas aeruginosa*, methicillin-resistant *S. aureus* (MRSA), and vancomycin-resistant *Enterococcus faecalis* (VRE). The antibacterial activity of both composites increases with the Ag^+ or Ag^0 content in the composites. More importantly, for the same bacteria and the same silver content, the [CEL+KER+AgClNPs] composite is relatively more toxic than [CEL+KER+Ag^0NPs] composite. Experimental results confirm that there was hardly any Ag^0NPs release from the [CEL+KER+Ag^0NPs] composite, and hence its antimicrobial activity and

ACS Applied materials & Interfaces, Vol 8, No. 50 (2016): pg. 34791-34801. DOI.

biocompatibility is due not to any released Ag^0NPs but rather entirely to the Ag^0NPs embedded in the composite. Both AgClNPs and Ag^0NPs were found to be toxic to human fibroblasts at higher concentration (>0.72 mmol), and for the same silver content, the [CEL+KER+AgClNPs] composite is relatively more toxic than the [CEL+KER+Ag^0NPs] composite. As expected, by lowering the Ag^0NPs concentration to 0.48 mmol or less, the [CEL+KER+Ag^0NPs] composite can be made biocompatible while still retaining its antimicrobial activity against bacteria such as *E. coli*, *S. aureus*, *P. aeruginosa*, MRSA, and VRE. These results, together with our previous finding that [CEL+KER] composites can be used for the controlled delivery of drugs such as ciprofloxacin, clearly indicate that the [CEL+KER+Ag^0NPs] composite possesses all of the required properties for it to be successfully used as a high-performance dressing to treat chronic ulcerous infected wounds.

Keywords: antibacteria, biocompatible, cellulose, ionic liquid, keratin, silver nanoparticles

Introduction

Interest in nanoparticles (NPs), particularly silver nanoparticles (AgNPs), has increased significantly recent years because, among other unique features, NPs are known to exhibit both antimicrobial and antiviral activities.[1-8] It has been shown that AgNPs exhibit highly antimicrobial activity against both Gram-positive and -negative bacteria.[1-8] They have also shown to be effective antiviral agents.[1-9] The size, morphology, and stability of NPs are known to strongly affect their antimicrobial and antiviral activity.[1-8] Colloidal NPs are known to undergo coagulation and aggregation in solution, which, in turn, lead to changes in their size and morphology and, hence, their antibacterial and antiviral properties. It is, therefore, important to develop an effective and reliable method to anchor the NPs to a supporting material in order to prevent their coagulation and aggregation, so that they can maintain their activity. In fact, AgNPs have been encapsulated in various man-made polymers and/or biopolymers, and such systems have been reported to retain some of their antimicrobial and antiviral activity.[1-18] For example, anchoring AgNPs to methacrylic acid copolymer beads has proven to be highly effective against a few bacteria.[1-18] However, the antimicrobial properties of all reported AgNP-encapsulated composites were tested for only a very few bacteria, and, more importantly, their biocompatibility has not been determined.[1-18] The lack of the latter information is critical because toxicity of AgNPs is known to be dependent on the concentration, and without information on the biocompatibility, the application of such a

ACS Applied materials & Interfaces, Vol 8, No. 50 (2016): pg. 34791-34801. DOI.

composite is rather limited. It is, therefore, of particular importance to develop a novel method to anchor AgNPs to composite biopolymers such as cellulose (CEL) and keratin (KER) and thoroughly and systematically investigate the antimicrobial and biocompatibility of the composites.

KERs are a group of cysteine-rich fibrous proteins found in filamentous or hard structures such as hairs, wools, feathers, nails, and horns.[19-28] KER possesses amino acid sequences similar to those found on an extracellular matrix (ECM), and because ECM is known to interact with integrins, which enable it to support cellular attachment, proliferation, and migration, KER-based materials are expected to have such properties as well.[19-28] Furthermore, KER is known to possess advantages for wound care, tissue reconstruction, cell seeding and diffusion, and drug delivery.[11-20] Unfortunately, in spite of its unique properties, KER has relatively poor mechanical properties, and as a consequence, it was not possible to fully exploit the unique properties of KER for various applications.[19-28] To increase the structural strength of KER-based materials, attempts have been made to cross-link KER chains with a cross-linking agent or introduce functional groups to its amino acid residues via chemical reaction(s).[19-28] The rather complicated, costly, and multistep process is not desirable because it may inadvertently alter its unique properties, making the KER-based materials less biocompatible and toxic and removing or lessening its unique properties. A new method that can improve the structural strength of KER-based products not by synthetic methods but rather by the use of naturally occurring polysaccharides such as CEL is particularly needed.

We have demonstrated recently that a simple ionic liquid (IL), butylmethylimmidazolium chloride ([$BMIm^+Cl^-$]), can dissolve both CEL and KER, and by using this IL as the sole solvent, we developed a simple, green, and totally recyclable method to synthesize [CEL+KER] composites just by dissolution without using any chemical modifications or reactions.[29-35] Spectroscopy [Fourier transform infrared (FTIR), near-infrared (NIR), and cross-polarization magic angle spinning (CP-MAS) ^{13}C NMR] results indicate that there was no chemical alteration in the structures of CEL and KER.[29-35] While there may be some changes in the molecular weights of CEL and KER, by

ACS Applied materials & Interfaces, Vol 8, No. 50 (2016): pg. 34791-34801. DOI.

using newly developed partial least-squares regression to analyze the FTIR spectra of the [CEL+KER] composites, we found that KER retains some of it secondary structure in the composites.[31,35] The [CEL+KER] composites obtained were found to retain unique properties of their components, namely, superior mechanical strength from CEL and controlled release of drugs by KER.[29-35]

The information presented clearly indicates that it is possible to use [CEL+KER] as a biocompatible composite to encapsulate AgNPs. Such considerations prompted us to initiate this study, which aims to hasten the breakthrough by systematically exploiting the advantages of ILs, a green solvent, to develop a novel, simple method to synthesize the [CEL+KER] composite containing silver in either Ag^+ or Ag^0 forms. As will be demonstrated, by initially introducing silver salt into the [CEL+KER] composite during the dissolution of CEL and KER by [$BMIm^+Cl^-$] and subsequently reducing Ag^+ to Ag^0NPs directly in the composite, we successfully synthesize the [CEL+KER+Ag^0NPs] composite. Alternatively, by not carrying out the reduction reaction, we can obtain the [CEL+KER+Ag^+NPs] composite. Because the [CEL+KER+Ag^0NPs] and [CEL+KER+Ag^+NPs] composites obtained can keep the Ag^+NPs and Ag^0NPs from changing size and morphology as well as undergoing coagulation, they can, therefore, fully retain the unique property of the AgNPs for repeated use without any complication of the reducing activity and not fully recover after each use. With these two composites, we will be able to finally address the important question that, to date, still remains unanswered, namely, the antimicrobial activity of AgNPs due to either Ag^+ or Ag^0 or both, and if both forms are active, which NPs have higher activity. We will also systematically investigate the biocompatibility of the two composites; information obtained will be used to guide the selection and use of the NP composites. The synthesis, characterization, antimicrobial activity, and biocompatibility of the [CEL+KER+Ag^+NPs] and [CEL+KER+Ag^0NPs] composites are reported herein.

ACS Applied materials & Interfaces, Vol 8, No. 50 (2016): pg. 34791-34801. DOI.

Experimental Section

Chemicals

Microcrystalline cellulose (CEL; DP ≈ 300) and AgCl were from Sigma-Aldrich and were used as received. Raw (untreated) sheep wool, obtained from a local farm, was cleaned by Soxhlet extraction using a 1:1 (v/v) acetone/ethanol mixture at 80 ± 3 °C for 48 h. The wool was then rinsed with distilled water and dried at 100 ± 1 °C for 12 h.[30-32] 1-Methylimidazole and *n*-chlorobutane (both from Alfa Aesar, Ward Hill, MA) were distilled and subsequently used to synthesize [$BMIm^+Cl^-$] using a method previously reported.[19-35] Nutrient broth (NB) and nutrient agar (NA) were obtained from VWR (Radnor, PA). Minimal essential medium (MEM), fetal bovine serum (FBS), and penicillin–streptomycin were obtained from Sigma-Aldrich (St. Louis, MO), whereas Dulbecco's modified Eagle medium (DMEM), phosphate-buffered saline, and a trypsin solution (Gibco) were obtained from Thermo Fischer Scientific (Waltham, MA). CellTiter 96 AQueous One Solution Cell Proliferation Assay was obtained from Promega (Madison, WI).

Bacterial and Cell Cultures

The bacterial cultures used were obtained either from the American Type Culture Collection (ATCC, Rockville, MD) or from the Leibniz Institute DSMZ, German Collection of Microorganisms and Cell Cultures (Braunschweig, Germany). The cell cultures of human fibroblasts were obtained from ATCC (Rockville, MD).

Synthesis

[CEL+KER+Ag^+NPs] and [CEL+KER+Ag^0NPs] composites were synthesized with minor modification to the procedure that we developed previously for the synthesis of [CEL+CS+KER] composites.[30-32,35] As shown in Scheme 1, washed wool was dissolved in $BMIm^+Cl^-$ at 120 °C. Once dissolved, the solution temperature was reduced to 90 °C before CEL was added to the KER solution. Using this procedure, [$BMIm^+Cl^-$] solutions of CEL and KER containing up to a

ACS Applied materials & Interfaces, Vol 8, No. 50 (2016): pg. 34791-34801. DOI.

total concentration of 6 wt % (relative to the IL) with various compositions and concentrations were prepared. Concurrently, in a separate flash, AgCl was dissolved in 2 mL of [$BMIm^+Cl^-$], and the mixture will then be added dropwise to the $BMIm^+Cl^-$ solution of [CEL+KER]. The resulting solution was then cast onto poly(tetrafluoroethylene) (PTFE) molds with the desired thickness on Mylar films to produce thin composite films with different compositions and concentrations of CEL, KER, and Ag^+. They were then kept in the dark and at room temperature for 24 h to allow gelation to yield gel films. The Ag^+-doped gel film was then washed with water for 3 days to remove $BMIm^+Cl^-$ and then dried slowly (3–5 days) in the dark at room temperature in a humidity-controlled chamber to yield a [CEL+KER+Ag^+NPs] composite. Alternatively, the Ag^+-doped gel film was reduced with $NaBH_4$ to Ag^0NPs. For example, the gel film, sandwiched between two PTFE meshes, was placed in an aqueous solution of $NaBH_4$ either in the dark and at room temperature for 48 h. Subsequently, the reduced film was washed and dried slowly (~3–5 days) in the dark and at room temperature in a humidity-controlled chamber to yield a [CEL+KER+Ag^0NPs] composite.

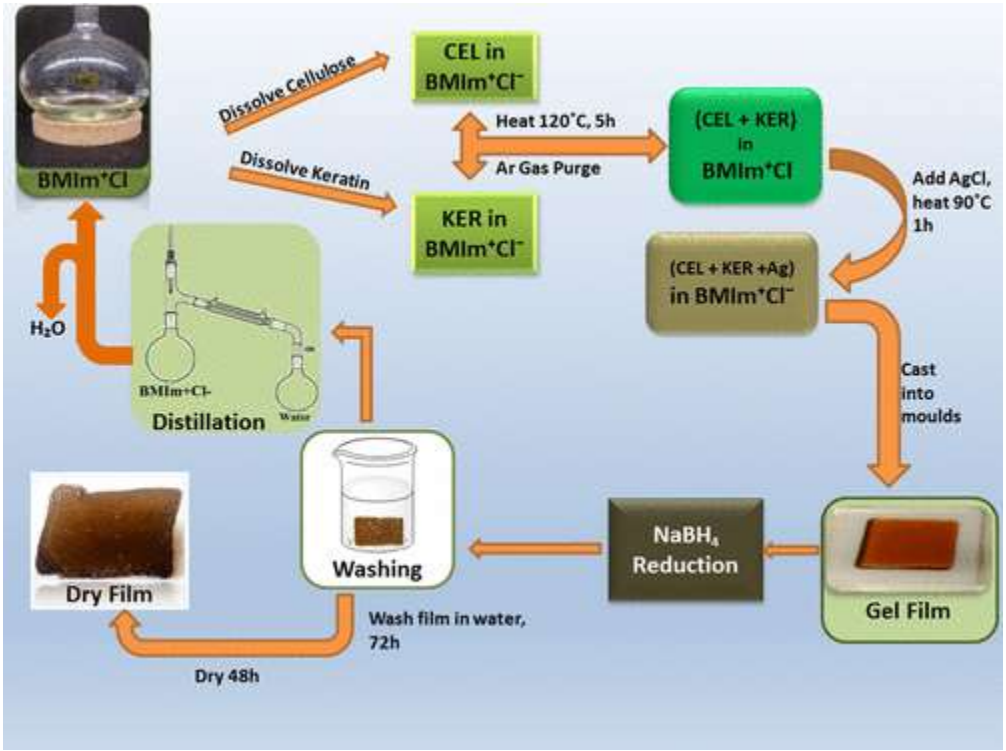

Scheme 1

ACS Applied materials & Interfaces, Vol 8, No. 50 (2016): pg. 34791-34801. DOI.

Analytical Characterization

FTIR spectra (from 450 to 4000 cm^{-1}) were recorded on a Spectrum 100 series FTIR spectrometer (PerkinElmer, USA) at a resolution of 2 cm^{-1} by the KBr method. Each spectrum was an average of 64 individual spectra. X-ray diffraction (XRD) measurements were taken on a Rigaku MiniFlex II diffractometer utilizing nickel-filtered Cu Kα radiation (1.54059 Å). The voltage and current of the X-ray tube were 30 kV and 15 mA, respectively. The samples were measured within the 2θ angle range from 2.0 to 40.00°. The scan rate was 5°/min. Data processing procedures were performed with the *Jade 8* program package.[29-35] The surface and cross-sectional morphologies of the composite films were examined under a vacuum with a JEOL JSM-6510LV/LGS scanning electron microscope with standard secondary electron (SEI) and backscattering electron (BEI) detectors. Prior to scanning electron microscopy (SEM) examination, the film specimens were made conductive by applying a 20 nm gold–palladium coating to their surfaces using an Emitech K575x Peltier-cooled sputter coater (EMI-Tech Products, Timpson, TX).

In Vitro Antibacterial Assays

The antibacterial characteristics of the newly synthesized composites were tested against *Escherichia coli* (ATCC 8739, DSMZ 498), *Staphylococcus aureus* (ATCC 25923, DSMZ 1104), methicillin-resistant *S. aureus* (ATCC 33591, DSMZ 11729), vancomycin-resistant *Enterococcus faecalis* (ATCC 51299, DSMZ 12956), and *Pseudomonas aeruginosa* (ATCC 9027, DSMZ 1128) using previously published protocol.[29,33,34] The cultures were grown in a sterile NB medium overnight at 37 °C and 150 rpm. Composites of dimensions of 3 × 20 mm were prior to the assay thermally sterilized at 121 °C and 15 psi for 20 min. They were placed in a diluted overnight culture (2 μL of overnight culture in 2 mL of NB) and incubated for 24 h at 37 °C and 200 rpm. Bacteria were plated in serial dilutions onto sterile NA plates at time 0 and after 24 h and incubated overnight at 37 °C. Colony-forming units (CFUs) were quantified on statistically significant plates (30–300 CFUs) and compared to a control (no added material). The log of reduction of bacteria was calculated for each experiment as follows:

ACS Applied materials & Interfaces, Vol 8, No. 50 (2016): pg. 34791-34801. DOI.

$$\log \text{ of reduction} = \log \frac{N_0}{N_t}$$

where N_0 is the number of bacteria at the beginning of the experiment and N_t is the number of bacteria after 24 h.

In Vitro Biocompatibility Assays

The biocompatibility of [AgNPs@CEL:KER] composites was assessed by the adherence and growth of fibroblasts in the presence of the composites, as previously reported.[29,33,34] Human fibroblasts (ATCC CRL-2522 or ATCC CCL-186) were grown in a sterile MEM or in a sterile DMEM supplemented with 10% FBS and 1% penicillin–streptomycin according to ATCC guidelines. The inoculated culture was grown at 37 °C in a humified atmosphere of 5% CO_2 until the third passage. Between passages, cells at approximately 80% confluency were subjected to trypsinization and recovered by centrifugation at 1000*g* for 10 min. The cell pellets were resuspended homogeneously in the culture media and transferred to a 75 cm^2 tissue culture flask for further passages. Cells were seeded in the wells of the 24-well plate at a concentration of 2×10^4 cells/mL and left for 1 day to allow for their attachment (approximately 50% confluency). Circle-shaped composites with either 15 or 7 mm diameter were autoclaved at 121 °C and 15 psi for 20 min and placed in the wells with attached cells the following day. Some wells contained cells without any added material and served as a control. After incubation for 3 days, that viability and fitness of the cells were evaluated both with a colorimetric CellTiter 96 AQueous One Solution Cell Proliferation Assay and visually with an Olympus DP12 digital microscope camera. The procedure as specified in the manufacturer's manual for the CellTiter 96 AQueous One Solution Cell Proliferation Assay was followed. In brief, the MTS reagent was added in a 1:5 ratio to each well after the medium in the wells was supplemented with a colorless MEM or DMEM. The cells were then incubated at standard culture conditions for 3 h. Then 100 μL from each well was transferred to a new 96-well cell culture plate, and the optical density (OD) value of the extracted supernatant was measured with a PerkinElmer HTS 7000 Bio Assay Reader at 490 nm. The percent viability was calculated using the following equation:

ACS Applied materials & Interfaces, Vol 8, No. 50 (2016): pg. 34791-34801. DOI.

$$\% \text{ cell viability} = \frac{\text{OD}_{\text{test sample}}}{\text{OD}_{\text{control}}} \times 100$$

where $OD_{test\ sample}$ is the measured OD at 490 nm of the extract from the test sample well and $OD_{control}$ is the measured OD at 490 nm of the extract from the control well.

Statistical Analysis

All experiments had a sample size of $n = 3$ and are representative of repeated trials. Sample error bars on the plots represent ± standard error of mean, where applicable. Tests for the statistical significance of the difference of the means were performed using a two-tailed Student's *t* test assuming unequal variances using Microsoft Office Excel. *P* values are indicated as follows in the figures: *, $P < 0.05$; **, $P < 0.005$; ***, $P < 0.001$.

Results and Discussion

FTIR

The FTIR spectrum of the [CEL+KER+Ag^0NPs] composite is presented as the green spectrum in Figure 1. For reference, the spectrum of the [CEL+KER] composite is also added (blue spectrum). As expected, the blue spectrum of [CEL+KER] is similar to those previously observed for the [CEL+KER] composites, namely, bands at 1700–1600 and 1550 cm^{-1} are due to C═O stretch (amide I) and C–N stretch (amide II) vibrations and those at 1300–1200 cm^{-1} are from the in-phase combination of the N–H bend and C–N stretch vibrations (amide III).[30-32,36-38] Major bands between 1200 and 900 cm^{-1} are due to sugar ring deformations of the CEL.[30-32,36-38] The fact that the green spectrum of the [CEL+KER+Ag^0NPs] composite is relatively similar to the blue spectrum of the [CEL+KER] composite seems to indicate that there may not be strong interaction between the Ag^0NPs and CEL and KER in the composite. However, careful inspection of the spectra revealed that there are indeed minor differences in the amide bands at around 1700–1600 and 1550 cm^{-1} between the two spectra. Specifically, interaction between the Ag^0NP and the C═O group leads to

ACS Applied materials & Interfaces, Vol 8, No. 50 (2016): pg. 34791-34801. DOI.

a shift in the amide band from 1650 cm^{-1} (of the [CEL+KER] composite) to 1655 cm^{-1} (of the [CEL+KER+ Ag^0NP] composite). Also, the small shoulder at ~1449 cm^{-1} disappears upon the addition of Ag^0NP to the composite. These results seem to indicate that there may be some interactions between the Ag^0NP and the amide groups of the KER. Furthermore, the difference of the band at ~2870 cm^{-1} between the spectra of the two composites suggests that there may be some modifications in the hydrogen bonding when the Ag^0NP was incorporated into the [CEL+KER] composite.[30-32]

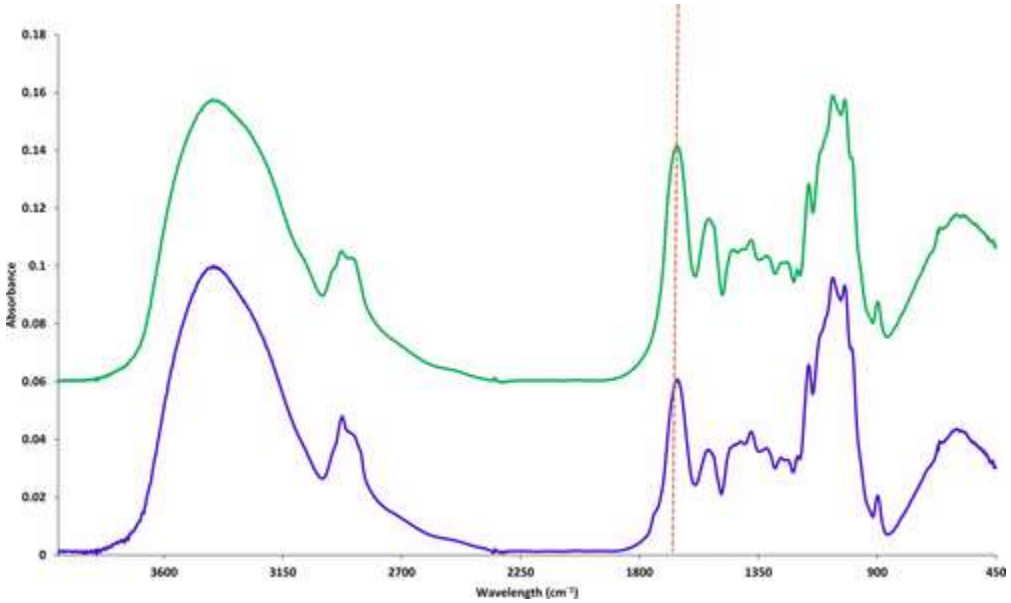

Figure 1. FTIR spectra of the [CEL+KER] (blue) and [CEL+KER+AgNPs] (green) composites.

Powder XRD

X-ray diffractograms of [CEL+KER+Ag^+NPs] and [CEL+KER+Ag^0NPs] composites are shown in Figure 2. Because CEL and KER are present in both composites, it is expected that both spectra have two similar broad bands at around 2θ = 10.75° and 20.85°, which are due to CEL and KER. Because the valency of the AgNPs is different in the composites, narrow crystalline bands that are due to the AgNPs are distinctly different for the two composites. Specifically, the diffractogram of the [CEL+KER+Ag^+NPs] composite (blue spectrum) exhibits three major peaks at 2θ = 27.94°, 32.35°, and 46.37°, which are characteristic of the (1 1 1), (2 0 0), and (2 2 0) peaks, respectively, of silver chloride nanoparticles (AgClNPs).[39-43]

ACS Applied materials & Interfaces, Vol 8, No. 50 (2016): pg. 34791-34801. DOI.

The fact that these peaks are the same as those previously reported for AgClNPs[40-43] as well as the reference diffractogram of AgCl reported in the JCPDS 31-1238 seems to indicate that Ag^+ is present in the form of AgCl nanoparticles in the composite. It is hardly surprising that AgCl NPs are present in the [CEL+KER+Ag^+] composites. This is because, as described in the Experimental Section, AgCl was used as the source for Ag^+ during the synthesis of the composites. Because AgCl is completely soluble in [$BMIm^+Cl^-$], it was initially dissolved in the IL and then added to the [$BMIm^+Cl^-$] solution of [CEL+KER]. It seems that when the [CEL+KER+Ag^+] film underwent gelation and subsequently washing with water to remove [$BMIm^+Cl^-$] from the film, Ag^+ recombined with Cl^- to form the AgCl NPs. The presence of excess chloride ion from [$BMIm^+Cl^-$] further promotes forming of AgCl NPs from Ag^+ as well.

Conversely, the diffraction peaks at 38.47°, 44.57°, 64.87°, and 77.66° in the orange spectrum of the [CEL+KER+Ag^0NPs] composite can be attributed to the (1 1 1), (2 0 0), (2 2 0), and (3 1 1) bands of Ag^0.[44-46] The fact that there is no diffraction peak of Ag^0 in [CEL+KER+Ag^+NPs] suggests that this composite contains only AgClNPs. Similarly, because no peak due to AgClNPs is seen in the diffractogram of the [CEL+KER+Ag^0NPs] composite, it is reasonable to infer that silver ion was completely reduced to metallic AgNPs during the synthesis.

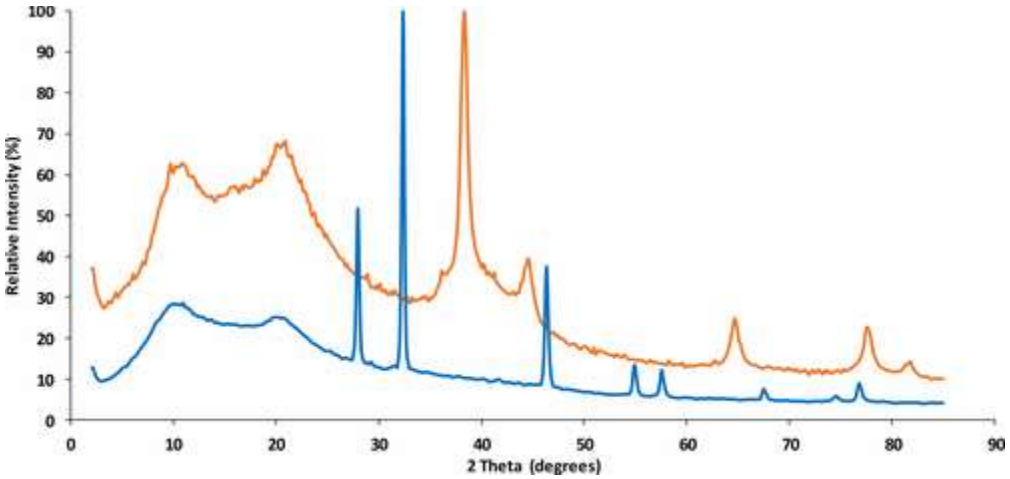

Figure 2. Powder XRD spectra of the [CEL+KER+Ag^+NPs] (blue) and [CEL+KER+Ag^0NPs] (orange) composites.

The Scherrer equation was then used to determine the size (τ value) of the AgClNPs and Ag^0NPs in the composites from the full width

at half-maximum (fwhm; β value in the equation) of their corresponding XRD peaks:[47,48]

$$\tau = \frac{k\lambda}{\beta \cos\theta}$$

where τ is the size of the NP, λ is the X-ray wavelength, and *k* is a constant.[31,32] The size of the metallic AgNP in the [CEL+KER+Ag^0] composite was found to be 9 ± 1 nm, while the AgClNP in the [CEL+KER+Ag^+] composite has a size of 27 ± 2 nm. It is unclear why the size of the silver chloride is much larger than that of the metallic AgNP. It may be possible that the stirring and reduction with $NaBH_4$ further dispersed the AgNPs in the [CEL+KER] composite, thereby preventing them from coagulation upon reduction to Ag^0NPs.

SEM Images and Energy-Dispersive Spectroscopy (EDS) Analysis

Shown in Figure 3A are the surface (left) and cross-sectional SEM images of the [CEL+KER+Ag^0NPs] composite. As expected, the images of the composite are similar to those previously observed for the [CEL+KER] composites.[30-32] That is, CEL and KER are homogeneously distributed throughout the composite. While CEL is known to have rather smooth structure, the presence of KER in the composite gives it a rough and porous structure with a three-dimensional interconnection throughout the film. More information on the chemical composition and homogeneity of the composite can be seen in Figure 3B,C, which show the EDS spectrum of the composite (part B) and images taken with an EDS detector specifically set for carbon (part C, left), silver (part C, center), and oxygen (part C, right). As is evident from the figures, the AgNPs not only were well-incorporated in the composites but also were present as well-distributed NPs throughout the composite.

ACS Applied materials & Interfaces, Vol 8, No. 50 (2016): pg. 34791-34801. DOI.

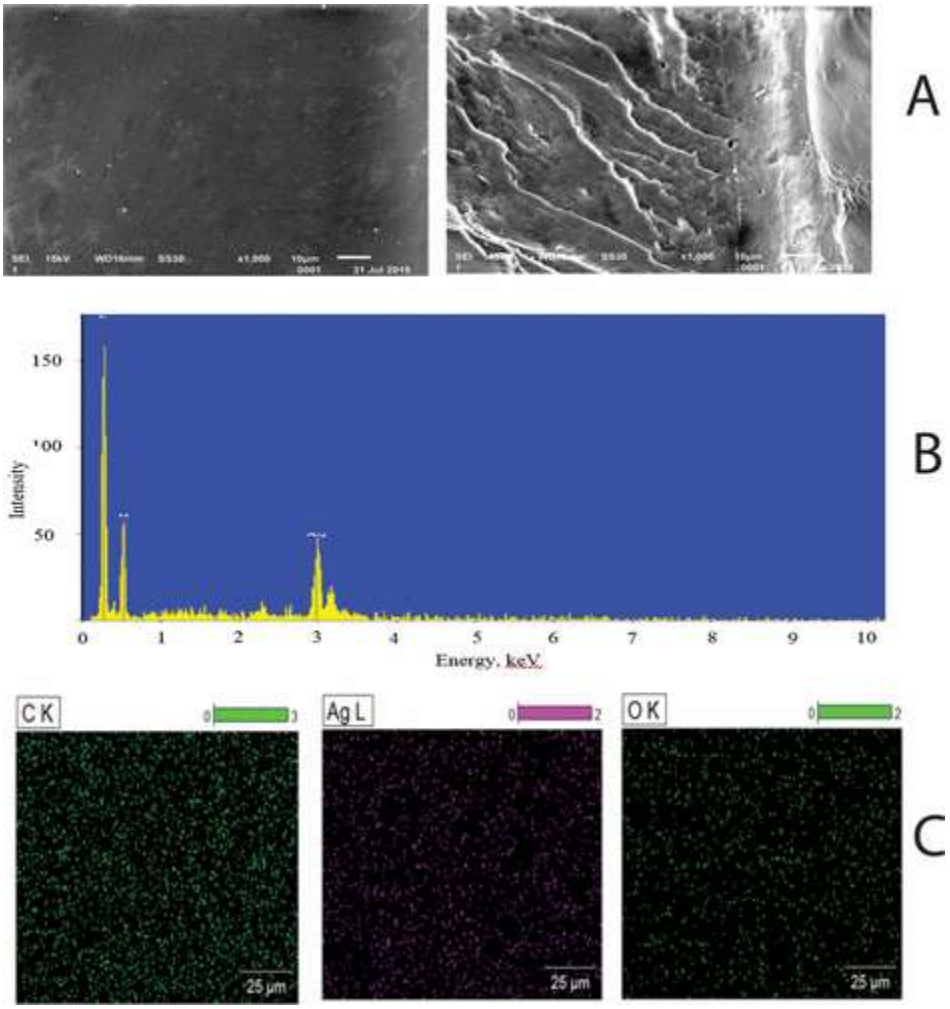

Figure 3. (A) SEM images of the [CEL+KER+AgNPs] composite: (left) surface image; (right) cross-sectional image. (B) EDS spectrum and (C) EDS images recorded for carbon (left), silver (middle), and oxygen (right) of the [CEL+KER+AgNPs] composite.

Antibacterial Assay

To assess the antimicrobial effect of AgNPs in the [CEL+KER+AgNPs] composites, bacteria were grown in the presence of the composites and then plated out onto NA and measured by the number of colonies formed compared to those for the blank ([CEL+KER] composite) and the control (no composite). Results for the microbial log of reduction of different composites are shown in Figure 4 in both the top (for composites with 3.5 mmol of either Ag^{+} or Ag^{0}) and bottom (for NPs with three different concentrations: 3.5, 0.72, and 0.48 mmol). It is evident that the bactericidal activity of the [CEL+KER+AgNPs] composites increases with the concentration of

ACS Applied materials & Interfaces, Vol 8, No. 50 (2016): pg. 34791-34801. DOI.

AgNPs in both Ag^0 and Ag^+ forms for all bacteria tested. Specifically, as shown in Figure 4, top, the [CEL+KER+Ag^0] composites (blue bar) with 3.5 mmol of silver exhibited the highest bactericidal activity against all selected bacteria with up to 6 logs of reduction in the number of bacteria, which corresponds to a 99.9999% growth reduction. Even at a silver concentration of as low as 0.48 mmol, the composite still exhibited up to 0.5 logs of reduction, or a 68% growth reduction for most of bacteria, with the exception of VRE, where 1 log of reduction was observed (Figure 4, bottom). As expected, the controls and blank samples (yellow bar) did not exhibit any statistically significant reduction in the number of bacteria, and there was no significant difference between them.

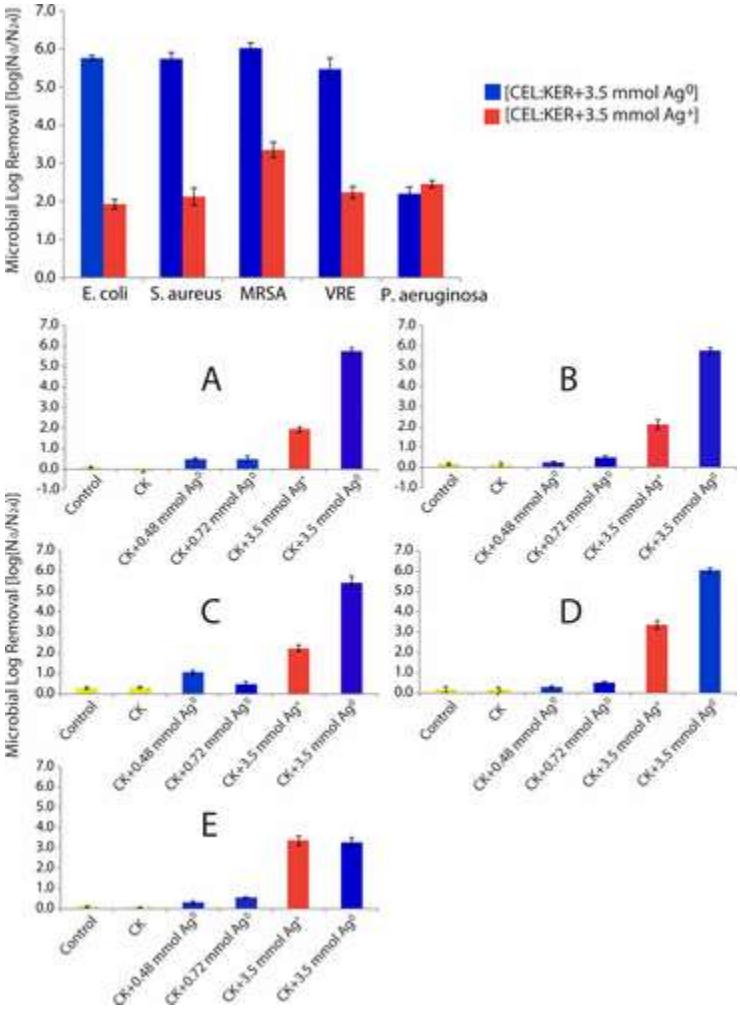

Figure 4. Log of growth reduction for *E. coli*, *S. aureus*, VRE, MRSA, and *P. aeruginosa* after 24 h of exposure to (top) [CEL+KER+Ag^+NPs] and [CEL+KER+Ag^0NPs] composites with a AgNP concentration of 3.5 mmol and (bottom) [CEL+KER+Ag^+NPs] and [CEL+KER+Ag^0NPs] composites with AgNP concentrations of

ACS Applied materials & Interfaces, Vol 8, No. 50 (2016): pg. 34791-34801. DOI.

3.5, 0.72, and 0.48 mmol for (A) *E. coli*, (B) *S. aureus*, (C) VRE, (D) MRSA, and (E) *P. aeruginosa*. In these figures, CEL+KER was labeled as CK; red and blue bars are for the [CEL+KER+Ag^+] and [CEL+KER+Ag^0NPs] composites, respectively. Yellow bars are for both the blank ([CEL+KER] composite with no AgNPs) and control. See the text for detailed information.

While it is known that AgNPs are bactericidal, to date, it is still unclear if the antimicrobial activity is due to Ag^0 or Ag^+ (as in AgCl). As described above, by the judicious selection of the synthetic method, [CEL+KER+AgNPs] can be synthesized with the AgNPs in either Ag^0 or Ag^+ form. This makes it possible, for the first time, to elucidate the mechanism of the antimicrobial activity of AgNPs. Accordingly, microbial assays were carried out in the presence of either [CEL+KER+Ag^0NPs] (blue bars) or [CEL+KER+Ag^+] (red bars) composites. The results obtained, shown in both the top and bottom of Figure 4, clearly show that, for the same bacteria and the same silver content, the [CEL+KER+Ag^0] composites (blue bar) exhibit relatively greater antimicrobial activity against bacteria compared to the corresponding [CEL+KER+Ag^+] composites (red bars). For example, as shown in the bottom of Figure 4A–D, up to 6 logs of reduction of growth was found by the [CEL+KER+Ag^0NPs] composite for all four bacteria (*E. coli*, *S. aureus*, MRSA, and VRE), whereas the [CEL+KER+ Ag^+] composite exhibits only a 3.5 log of reduction. Surprisingly, within experimental error, there was no significant difference between these two NP composites for *P. aeruginosa* (Figure 4E). The results obtained also indicate not only that the [CEL+KER+Ag^0NPs] composites have relatively stronger antimicrobial activity compared to the corresponding [CEL+KER+Ag^+] composites but also that the rather limited antimicrobial activity of the latter cannot be enhanced by increasing the concentration of Ag^+ in the composites because, as will be shown in the following section, Ag_2^+ is not biocompatible and, as a consequence, increasing the Ag^+ concentration would undesirably lead to the damaging and killing of human cells. Again, as expected, there was no statistically significant decrease in the number of bacteria after 24 h in the control experiments (no composite) and blank samples.

Biocompatibility Assay

To assess the potential cytotoxicity of the [CEL+KER+AgNPs] composites with different concentrations of AgNPs, the morphology and proliferation capability of adherent human fibroblasts in the

ACS Applied materials & Interfaces, Vol 8, No. 50 (2016): pg. 34791-34801. DOI.

presence or absence of NP composites were analyzed. The proliferation capability was assessed using a CellTiter 96 AQueous Non-Radioactive Cell Proliferation Assay (or CellTiter 96 AQueous One Solution Cell Proliferation Assay) colorimetric assay, whereas the morphology of fibroblasts was examined microscopically. Three trials were performed for this assay, employing composites with different sizes (circles of either 15 or 7 mm diameter) and silver concentrations. Fibroblasts were exposed to the composites for 3 days. The proliferation and viability of fibroblasts in the presence or absence of composites with different concentrations of AgNPs over 3 days are shown in Figure 5. The statistical significance in the differences between the sample and control wells was evaluated with a two-tailed Student's *t* test, and the degree of significance is indicated with *P* values in different significance levels (α = 0.05, 0.005, or 0.001). In the first trial, the composites of 15 mm diameter with 3.5 mmol of either Ag^+ or Ag^0 concentration were tested (Figure 5A). The fibroblasts in contact with either the 3.5 mmol [CEL+KER+Ag^0] (blue bar) or the 3.5 mmol [CEL+KER+Ag^+] (red bar) exhibited low absorbances at 490 nm, indicating that the cells were not viable. Morphological data obtained through microscopic examination indicated that the fibroblasts in these wells were not attached and exhibit unusual round morphology (data not shown). This seems to indicate that the cells were not healthy and possibly not viable. To reduce the concentration of AgNPs in the composites, in the second trial, the diameter of the composites used was reduced from 15 to 7 mm, which corresponds to a 4.6 reduction in the area of the composites. As shown in Figure 5B, the cells in the sample wells exhibited slightly increased viability after 3 days compared to that in the first trial. Morphological data showed round unattached cells (data not shown). Because the results obtained so far indicate that the biocompatibility of the [CEL+KER+Ag^0] composites are relatively better than that of the corresponding [CEL+KER+Ag^+] composites, subsequent experiments were carried out using only the former. Specifically, [CEL+KER+Ag^0] composites with relatively lower Ag^0NP concentrations (0.48 and 0.72 mmol) were used (Figure 5C). In this case, the viability of the cells in the composite wells after 3 days of exposure was high, approximately 83% for 0.48 mmol of Ag^0NPs and (64 ± 5)% for 0.72 mmol of Ag^0NPs compared to the control. It is evidently clear that, within experimental error, there was no statistically significant difference between the cells in the wells of 0.72

ACS Applied materials & Interfaces, Vol 8, No. 50 (2016): pg. 34791-34801. DOI.

and 0.48 mmol of Ag^0NPs and those in the control well. Morphological data presented as images of cells in the 0.48 mmol of Ag^0NPs well (Figure 6C) and in the 0.72 mmol of Ag^0NPs well (Figure 6D) show a mix of healthy-looking cells and round unattached cells, similar to those observed for cells in the absence of composite (Figure 6A) and with the [CEL+KER] composite (Figure 6B). Taken together, the results clearly indicate that both Ag^+ and Ag^0NPs are toxic to human fibroblasts at higher concentration (>0.72 mmol). At the same concentration, Ag^+ is relatively more toxic than Ag^0. More importantly, at or below the silver concentration of 0.48 mmol, the [CEL+KER+Ag^0NPs] composite not only is fully biocompatible but also fully reatains its antimicrobial activity against bacteria such as *E. coli*, *S. aureus*, *P. aeruginosa*, MRSA, and VRE.

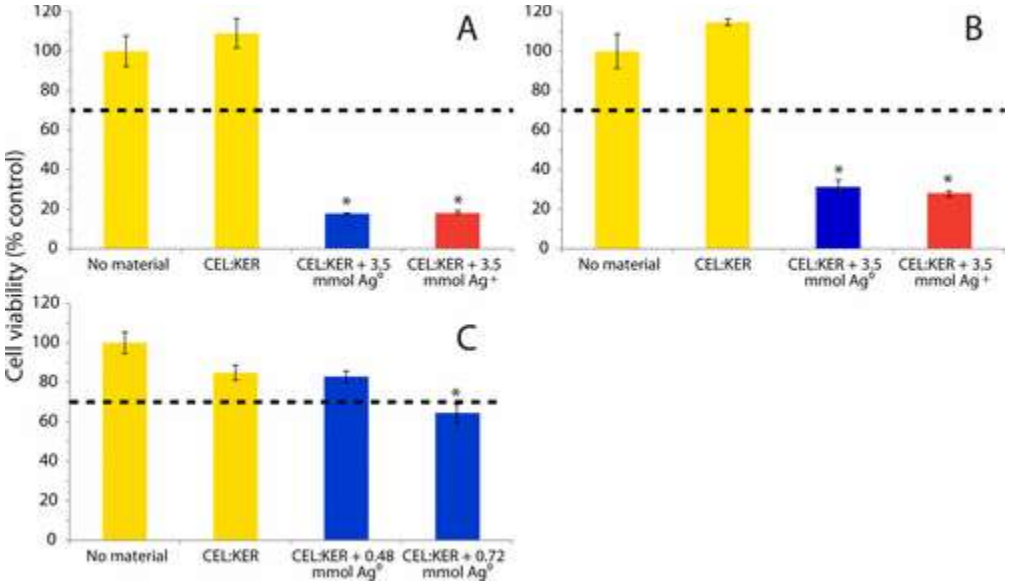

Figure 5. Fibroblast viability based on the absorbance at 490 nm after being exposed to the [CEL+KER] (yellow), [CEL+KER+Ag^0NPs] (blue), and [CEL+KER+Ag^+NPs] (red) composites for 3 days. In part A, composites of 15 mm diameter were used, and in parts B and C, the composites were of 7 mm diameter. Each bar represents an average of three experiments. Error bars represent standard errors of the average. *P* values are indicated as follows: *, $P < 0.05$. The results for the control experiment (no composite) are also presented as yellow bars. Composites causing <70% cell viability (dashed line) are considered cytotoxic.

ACS Applied materials & Interfaces, Vol 8, No. 50 (2016): pg. 34791-34801. DOI.

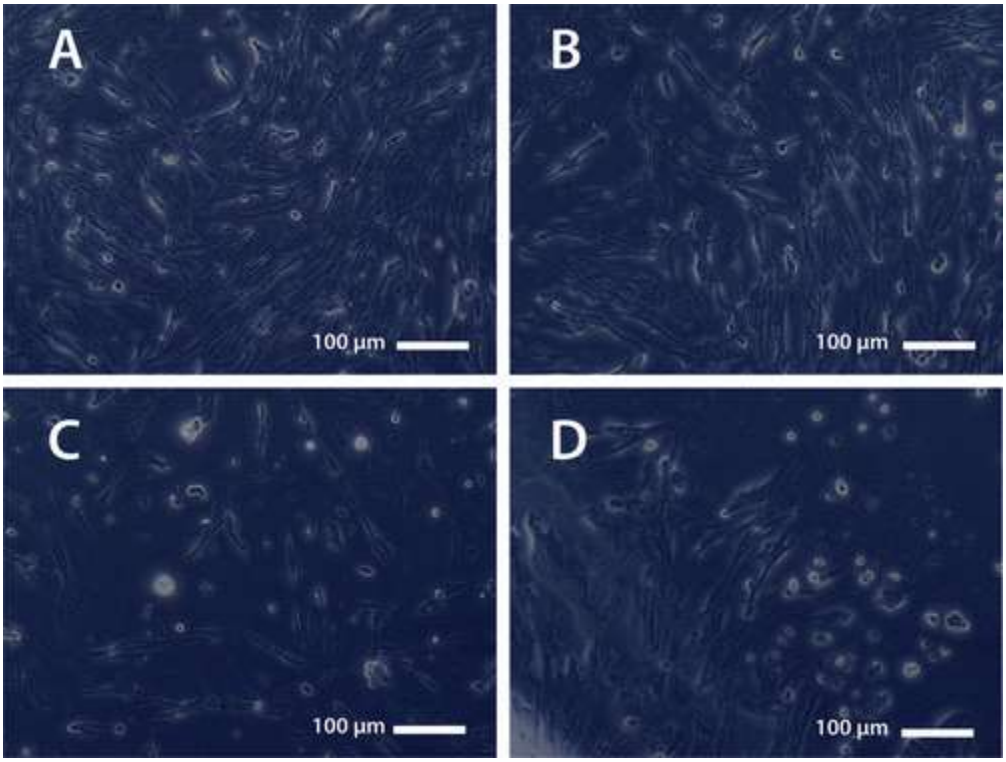

Figure 6. Images (100×) of human fibroblasts after 3 days in the absence of any composite (A), with the [CEL+KER] composite (B), with [CEL+KER] containing 0.48 mmol of Ag^0NPs (C), and with [CEL+KER] containing 0.72 mmol of Ag^0NPs (D).

Release of Ag^0NPs from the [CEL+KER+Ag^0NPs] Composites

We also carried out experiments to determine if any Ag^0NPs are leaking out from the [CEL+KER+Ag^0NPs] composites during the microbial and biocompatibility assays. Such information is particularly important because it would clarify the mechanism of the antibacterial activity and biocompatibility of the composites. That is, the activity is due to either Ag^0NPs in the composites and/or Ag^0NPs released from the composites. As described in the Experimental Section, because the [CEL+KER+Ag^0NPs] composites were exhaustively washed with water for a total of up to 10 days, it is expected that, if there is any leaking of AgNPs from the composites, their concentration should be extremely low. Accordingly, we used a modified version of the recently developed ultrasensitive method based on the thermal lens technique to determine the concentration of any possible leaking of Ag^0NPs from the composites during the bioassay.[49,50] No experiment was carried out

ACS Applied materials & Interfaces, Vol 8, No. 50 (2016): pg. 34791-34801. DOI.

to measure the release of Ag^+ form the [CEL+KER+Ag^+] composites because, compared to the [CEL+KER+Ag^0NPs] composites, the [CEL+KER+Ag^+] composites are not readily usable because they are not biocompatible and have relatively lower antimicrobial activity. This thermal lens detection method is so sensitive that it can detect released AgNPs at a concentration as low as 0.51 μg/L.[33] As described in detail in the Supporting Information, two different concentration values can be obtained from this method: the colloidal silver concentration or concentration of released Ag^0NPs and total silver concentration, which is the sum of the released Ag^0NPs concentration plus the released Ag^+ concentration. As described above, XRD results show that there is no Ag^+ in the [CEL+KER+Ag^0NPs] composites; i.e., all Ag^+ was reduced by $NaBH_4$ to Ag^0NPs during the preparation. However, there is a possibility that the concentration of Ag^+ remaining in the composites was so low that it cannot be detected by XRD. This thermal lens detection is so sensitive that it can detect any Ag^+ that is released from the Ag^+ remaining in the composites.

The results obtained are presented in Figure 7 and plotted as the concentration of released silver against the time that the composites were immersed in a solution similar to the media used in the microbial and biocompatibility assays. The fact that, within experimental error and at all times (from the beginning to 7 days), the obtained concentration of released Ag^0NPs (blue bars) was the same as that of the total concentration of released silver (red bars) clearly indicates that all released silver was Ag^0NPs and there was no Ag^+ released from the composites. Also, the concentrations of released Ag^0NPs after 3 days were the same, within experimental error, as those after 7 days indicate that no more Ag^0NPs was released beyond 3 days. More importantly, even after a plateau was reached at about 3 days and continued beyond 7 days, only 2.3 μg of Ag^0NPs was released from [CEL+KER+Ag^0NPs]. Because the total concentration of silver in the composite used in the measurements was about 12 mg, less than 0.02% of Ag^0NPs was released from the [CEL+KER+Ag^0NPs] composites even after they were soaked in the solution for 7 days. Taken together, the results obtained clearly indicate that there was hardly any Ag^0NPs release from the [CEL+KER+Ag^0NPs] composite, and hence its antimicrobial activity and biocompatibility are due not to

ACS Applied materials & Interfaces, Vol 8, No. 50 (2016): pg. 34791-34801. DOI.

any released Ag^0NPs but rather entirely to the Ag^0NPs embedded in the composite.

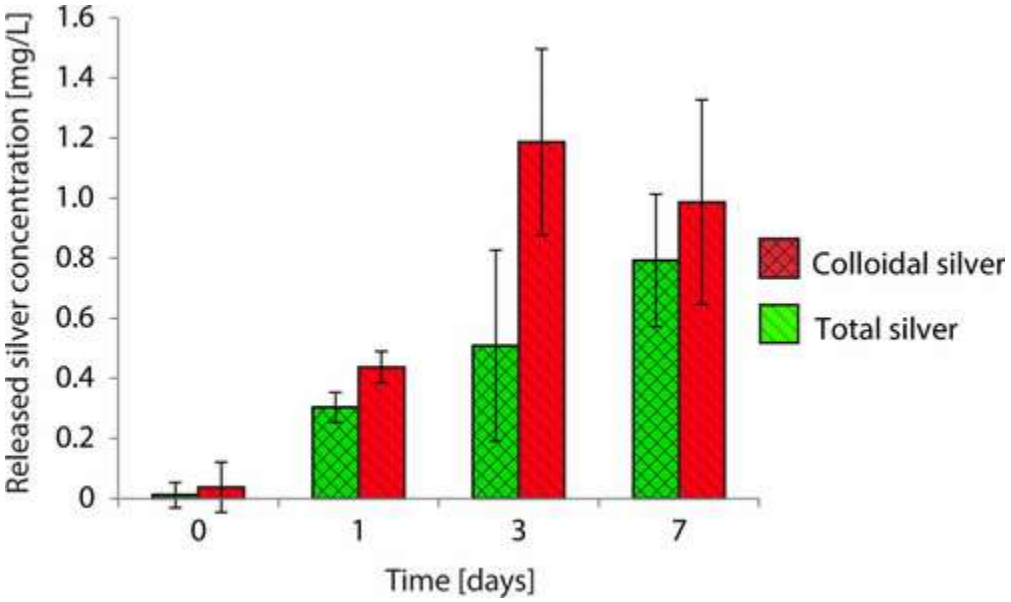

Figure 7. Plot of the concentration of AgNP released from the composites against the time that the composites were immersed in a solution similar to the media used in the microbial and biocompatibility assays. See the text for detailed information.

Conclusions

In summary, we have shown that biocompatible composites containing 50% CEL and 50% KER and silver of either ionic (Ag^+, presented as AgClNPs) or metallic (Ag^0NPs) were successfully synthesized in a simple process in which [$BMIm^+Cl^-$], a simple IL, was used as the sole solvent and AgCl was added to the [$BMIm^+Cl^-$] solution of [CEL+KER] during the dissolution process. The silver in the composite can be maintained as Ag^+ or completely converted to Ag^0NPs by reducing it with $NaBH_4$. The results of spectroscopy (FTIR and XRD) and imaging (SEM) measurements confirm that CEL and KER remain chemically intact and homogeneously distributed in the composites. The XRD and SEM results show that the silver in the [CEL+KER+Ag^+] and [CEL+KER+Ag^0] composites is homogeneously distributed throughout the composites in either AgClNPs or Ag^0NPs form with sizes of 27 ± 2 or 9 ± 1 nm, respectively. Both composites were found to exhibit excellent antibacterial activity against many bacteria including *E. coli*, *S. aureus*, *P. aeruginosa*, MRSA, and VRE. The bacterial activity of both composites increases with the Ag^+ or Ag^0NPs content in the composites. More importantly, for the same

ACS Applied materials & Interfaces, Vol 8, No. 50 (2016): pg. 34791-34801. DOI.

bacteria and the same silver content, the [CEL+KER+Ag^0NPs] composite exhibits relatively greater antimicrobial activity against bacteria compared to the corresponding [CEL+KER+Ag^+] composite. Experimental results confirm that there was hardly any Ag^0NPs released from the [CEL+KER+Ag^0NPs] composite, and hence its antimicrobial activity and biocompatibility are due not to any released Ag^0NPs but rather entirely to the Ag^0NPs embedded in the composite. Both Ag^+ and Ag^0NPs were found to be toxic to human fibroblasts at higher concentration (>0.72 mmol), and for the same silver content, the [CEL+KER+Ag^+] composite is relatively more toxic than the [CEL+KER+Ag^0NPs] composite. As expected, by lowering the Ag^0NPs concentration to 0.48 mmol or less, the [CEL+KER+Ag^0NPs] composite is biocompatible while still retaining its antimicrobial activity against bacteria such as *E. coli*, *S. aureus*, *P. aeruginosa*, MRSA, and VRE. These results, together with our previous finding that [CEL+KER] composites can be used for the controlled delivery of drugs such as ciprofloxacin, clearly indicate that the [CEL+KER+Ag^0NPs] composite possesses all the required properties for it to be successfully used as a high-performance dressing to treat chronic ulcerous infected wounds.

The authors declare no competing financial interest.

Acknowledgment

The authors are grateful to Prof. Raymond Fournelle for his competent assistance to measure SEM, Dr. Martina Bergant, Ph.D., for her assistance with the cell culture work at University of Nova Gorica, and Moven Mututuvari and James Makuvaza for their assistance. F.P. thanks the Fulbright Foundation for a fellowship supporting his time spent doing research at Marquette University. Research reported in this publication was supported by the National Institute of General Medical Sciences of the National Institutes of Health under Award R15GM099033.

References

[1]Yang, X.; Yang, M.; Pang, B.; Vara, M.; Xia, Y.Gold Nanomaterials at Work in *Biomedicine Chem. Rev.* 2015, 115, 10410– 10488, DOI: 10.1021/acs.chemrev.5b00193

[2]Xia, X.; Zeng, J.; Zhang, Q.; Moran, C. H.; Xia, Y.Recent Developments in Shape-Controlled Synthesis of Silver Nanocrystals *J. Phys. Chem. C* 2012, 116, 21647– 21656, DOI: 10.1021/jp306063p

[3]Chan, W. C. W.A Year for Nanoscience *ACS Nano* 2014, 8, 11901– 11903, DOI: 10.1021/nn5070716

[4]Pelaz, B.The State of Nanoparticle-Based Nanoscience and Biotechnology: Progress, Promises, and Challenges *ACS Nano* 2012, 6, 8468– 8483, DOI: 10.1021/nn303929a

[5]Sardar, R.; Shumaker-Parry, J. S.Spectroscopic and Microscopic Investigation of Gold Nanoparticle Formation: Ligand and Temperature Effects on Rate and Particle Size *J. Am. Chem. Soc.* 2011, 133, 8179– 8190, DOI: 10.1021/ja107934h

[6]Wang, Z.; Bharathi, M. S.; Hariharaputran, R.; Xing, H.; Tang, L.; Li, J.; Zhang, Y.-W.; Lu, Y.pH-Dependent Evolution of Five-Star Gold Nanostructures: An Experimental and Computational Study *ACS Nano* 2013, 7, 2258– 2265, DOI: 10.1021/nn305395p

[7]Wright, A. R.; Li, M.; Ravula, S.; Cadigan, M.; El-Zahab, B.; Das, S.; Baker, G. A.; Warner, I. M.Soft-and Hard-Templated Organic Salt Nanoparticles with the Midas Touch: Gold-Shelled NanoGUMBOS *J. Mater. Chem. C* 2014, 2, 8996– 9003, DOI: 10.1039/C4TC01006J

[8]Takagai, Y.; Miura, R.; Endo, A.; Hinze, W. L.One-pot Synthesis with in situ Preconcentration of Spherical Monodispersed Gold Nanoparticles using Thermoresponsive 3-(alkyldimethylammonio)-propyl sulfate Zwitterionic Surfactants *Chem. Commun.* 2016, 52, 10000– 10003, DOI: 10.1039/C6CC04584G

[9]Trefry, J. C.; Wooley, D. P.Silver Nanoparticles Inhibit Vaccinia Virus Infection by Preventing Viral entry through a Macropinocytosis-dependent Mechanism *J. Biomed. Nanotechnol.* 2013, 9, 1624– 1635, DOI: 10.1166/jbn.2013.1659

[10]Noh, H. J.; Im, A.-R.; Kim, H.-S.; Sohng, J. K.; Kim, C.-K.; Kim, Y. S.; Cho, S.; Park, Y.Antibacterial Activity and Increased Freeze-drying Stability of Sialyllactose-reduced Silver Nanoparticles using Sucrose and Trehalose *J. Nanosci. Nanotechnol.* 2012, 12, 3884– 3895, DOI: 10.1166/jnn.2012.6169

[11]Guzman, M.; Dille, J.; Godet, S.Synthesis and Antibacterial Activity of Silver Nanoparticles against Gram-positive and Gram-negative Bacteria *Nanomedicine* 2012, 8, 37– 45, DOI: 10.1016/j.nano.2011.05.007

[12]Mallakpour, S.; Dinari, M.; Talebi, M.A Facile, Efficient, and Green Fabrication of Nanocomposites based on L-leucine Containing Poly(amide-imide) and PVA-modified Ag Nanoparticles by Ultrasonic Irradiation Colloid *Colloid Polym. Sci.* 2015, 293, 1827– 1833, DOI: 10.1007/s00396-015-3581-0

[13]Gangadharan, D.; Harshvardan, K.; Gnanasekar, G.; Dixit, D.; Popat, K. M.; Anand, P. S.Polymeric Microspheres Containing Silver Nanoparticles as a Bactericidal Agent for Water Disinfection *Water Res.* 2010, 44, 5481– 5487, DOI: 10.1016/j.watres.2010.06.057

[14]Wei, D.; Sun, W.; Qian, W.; Ye, Y.; Ma, Y.The Synthesis of Chitosan-based Silver Nanoparticles and their Antibacterial Activity *Carbohydr. Res.* 2009, 344, 2375– 2382, DOI: 10.1016/j.carres.2009.09.001

[15]Johnston, J. H.; Nilsson, T.Nanogold and Nanosilver Composites with Lignin-containing Cellulose Fibres *J. Mater. Sci.* 2012, 47, 1103– 1112, DOI: 10.1007/s10853-011-5882-0

[16]Wu, J.; Zheng, Y.; Song, W.; Luan, J.; Wen, X.; Wu, Z.; Chen, X.; Wang, Q.; Guo, S.In situ Synthesis of Silver-Nanoparticles/bacterial Cellulose Composites for Slow-released Antimicrobial Wound Dressing *Carbohydr. Polym.* 2014, 102, 762– 771, DOI: 10.1016/j.carbpol.2013.10.093

[17]Kelly, F. M.; Johnston, J. H.Colored and Functional Silver Nanoparticle–Wool Fiber Composites *ACS Appl. Mater. Interfaces* 2011, 3, 1083– 1092, DOI: 10.1021/am101224v

[18]Boroumand, M. N.; Montazer, M.; Simon, F.; Liesiene, J.; Šaponjic, Z.; Dutschk, V.Novel Method for Synthesis of Silver Nanoparticles and their Application on Wool *Appl. Surf. Sci.* 2015, 346, 477– 483, DOI: 10.1016/j.apsusc.2015.04.047

[19]Hill, P.; Brantley, H.; Van Dyke, M.Some Properties of Keratin Biomaterials: Kerateines *Biomaterials* 2010, 31, 585– 593, DOI: 10.1016/j.biomaterials.2009.09.076

[20]Vasconcelos, A.; Cavaco-Paulo, A.The Use of Keratin in Biomedical Applications *Curr. Drug Targets* 2013, 14, 612– 619, DOI: 10.2174/1389450111314050010

[21]Sando, L.; Kim, M.; Colgrave, M. L.; Ramshaw, J. A.; Werkmeister, J. A.; Elvin, C. M.Photochemical Crosslinking of Soluble Wool Keratins Produces a Mechanically Stable Biomaterial that Supports Cell Adhesion and Proliferation *J. Biomed. Mater. Res., Part A* 2010, 95, 901– 911, DOI: 10.1002/jbm.a.32913

[22]Yamauchi, K.; Maniwa, M.; Mori, T.Cultivation of Fibroblast Cells on Keratin-coated Substrates *J. Biomater. Sci., Polym. Ed.* 1998, 9, 259– 270, DOI: 10.1163/156856298X00640

[23]Cui, L.; Gong, J.; Fan, X.; Wang, P.; Wang, Q.; Qiu, Y.Trans Glutaminase-modified Wool Keratin Film and its Potential Application in Tissue Engineering *Eng. Life Sci.* 2013, 13, 149– 155, DOI: 10.1002/elsc.201100206

[24]Xu, S.; Sang, L.; Zhang, Y.; Wang, X.; Li, X.Biological Evaluation of Human Hair Keratin Scaffolds for Skin Wound Repair and Regeneration *Mater. Sci. Eng., C* 2013, 33, 648– 655, DOI: 10.1016/j.msec.2012.10.011

[25]de Guzman, R. C.; Merrill, M. R.; Richter, J. R.; Hamzi, R. I.; Greengauz-Roberts, O. K.; Van Dyke, M. E.Mechanical and Biological Properties of Keratose Biomaterials *Biomaterials* 2011, 32, 8205– 8217, DOI: 10.1016/j.biomaterials.2011.07.054

[26]Iqbal, H. M.N.; Kyazze, G.; Locke, I. C.; Tron, T.; Keshavarz, T.In situ Development of Self-defensive Antibacterial Biomaterials: Phenol-g-keratin-EC based Biocomposites with Characteristics for Biomedical Applications *Green Chem.* 2015, 17, 3858– 3869, DOI: 10.1039/C5GC00715A

[27]Aluigi, A.; Vineis, C.; Varesano, A.; Mazzuchetti, G.; Ferrero, F.; Tonin, C.Structure and Properties of Keratin/PEO blend Nanofibers *Eur. Polym. J.* 2008, 44, 2465– 2475, DOI: 10.1016/j.eurpolymj.2008.06.004

[28]Khosa, M. A.; Ullah, A.A Sustainable Role of Keratin Biopolymer in Green Chemistry: A Review *J. Food Proc. Beverages* 2013, 1, 8– 15

[29]Rosewald, M.; Hou, F. Y. S.; Mutututuvari, T.; Harkins, A. L.; Tran, C. D.Cellulose-Chitosan-Keratin Composite Materials: Synthesis and Immunological and Antibacterial Properties *ECS Trans*. 2014, 64 (4) 499– 505, DOI: 10.1149/06404.0499ecst

[30]Tran, C. D.; Mutututuvari, T.Cellulose, Chitosan and Keratin Composite Materials. Controlled Drug Release *Langmuir* 2015, 31, 1516– 1526, DOI: 10.1021/la5034367

[31]Tran, C. D.; Mutututuvari, T.Cellulose, Chitosan and Keratin Composite Materials. Facile and Recyclable Synthesis, Conformation and Properties *ACS Sustainable Chem. Eng.* 2016, 4, 1850– 1861, DOI: 10.1021/acssuschemeng.6b00084

[32]Tran, C. D.; Prosenc, F.; Franko, M.; Benzi, G.Synthesis, Structure and Antimicrobial Property of Green Composites from Cellulose, Wool, Hair and Chicken Feather *Carbohydr. Polym.* 2016, 151, 1269– 1276, DOI: 10.1016/j.carbpol.2016.06.021

[33]Tran, C. D.; Duri, S.; Harkins, A. L.Recyclable Synthesis, Characterization and Antimicrobial Activity of Chitosan-based Polysaccharide Composite Materials *J. Biomed. Mater. Res., Part A* 2013, 101, 2248– 2257, DOI: 10.1002/jbm.a.34520

[34]Harkins, A. L.; Duri, S.; Kloth, L. C.; Tran, C. D.Chitosan-Cellulose Composite for Wound Dressing Material. Part 2. Antimicrobial Activity, Blood Absorption Ability and Biocompatibility *J. Biomed. Mater. Res., Part B* 2014, 102 (6) 1199– 1206, DOI: 10.1002/jbm.b.33103

[35]Mutututuvari, T. M., Supramolecular Biopolymeric Composite Materials: Green Synthesis, Characterization and Applications. Dissertation, Marquette University, Wilwaukee, WI, 2014.

[36]Li, R.; Wang, D.Preparation of Regenerated Wool Keratin Films from Wool Keratin-ionic liquid Solutions *J. Appl. Polym. Sci.* 2013, 127, 2648– 2653, DOI: 10.1002/app.37527

[37]Peplow, P. V.; Roddick-Lanzilotta, A. D. Orthopaedic Materials Derived from Keratin. U.S. Patent 2005/0232963 A1, 2005.

[38]Fang, J. Y.; Chen, J. P.; Leu, Y. L.; Wang, H. Y.Characterization and Evaluation of Silk Protein Hydrogels for Drug Delivery *Chem. Pharm. Bull.* 2006, 54, 156– 162, DOI: 10.1248/cpb.54.156

[39]JCPDS file No 31-1238.

[40]Dong, R.; Tian, B.; Zeng, C.; Li, T.; Wang, T.; Zhang, J.Ecofriendly Synthesis and Photocatalytic Activity of Uniform Cubic Ag@AgCl Plasmonic Photocatalyst *J. Phys. Chem. C* 2013, 117, 213– 220, DOI: 10.1021/jp311970k

[41]Veronica da Silva Ferreiraa, V. D. S.; ConzFerreiraa, M. E.; Lima, L. M. T. R. Green Production of Microalgae-based Silver Chloride Nanoparticles with Antimicrobial Activity against Pathogenic Bacteria *Enzym. Microbial. Tech.* 2016, Ahead of print: http://dx.doi.org/10.1016/j.enzmictec.2016.10.018.

[42]Dhas, T. S.; Kumar, V. G.; Karthick, V.; Angel, K. J.; Govindaraju, K.Facile Synthesis of Silver Chloride Nanoparticles using Marine Alga and its Antibacterial Efficacy, Spectrochim. Acta A Mol. Biomol. Spectrosc. *Acta A Mol. Biomol. Spectrosc.* 2014, 120, 416– 420

[43]Sohrabnezhad, Sh.; Rassa, M.; Dahanesari, E. M.Spectroscopic Study of Silver Halides in Montmorillonite and their Antibacterial Activity *J. Photochem. Photobiol., B* 2016, 163, 150– 155, DOI: 10.1016/j.jphotobiol.2016.08.018

[44]Sharma, P.; Sanpui, P.; Chattopadhyay, A.; Ghosh, S.Fabrication of Antibacterial Silver Nanoparticle—Sodium Alginate–Chitosan Composite Films *RSC Adv.* 2012, 2, 5837– 5843, DOI: 10.1039/c2ra00006g

[45]Sathishkumar, M.; Sneha, K.; Yun, Y. S.Immobilization of Silver Nanoparticles Synthesized using Curcuma Longa Tuber Powder and Extract on Cotton Cloth for Bactericidal Activity *Bioresour. Technol.* 2010, 101, 7958– 7965, DOI: 10.1016/j.biortech.2010.05.051

[46]JCPDS 04-0783.

[47]Scherrer, P.Bestimmung der Grösse und der Inneren Struktur von Kolloidteilchen Mittels Röntgenstrahlen, *Nachr. Ges. Wiss. Göttingen* 1918, 26, 98– 100

[48]Langford, J. J.; Wilson, A. J. C.Scherrer after Sixty Years: A Survey and Some New Results in the Determination of Crystallite Size *J. Appl. Crystallogr.* 1978, 11, 102– 113, DOI: 10.1107/S0021889878012844

[49]Korte, D.; Concetta Bruzzoniti, M.; Sarzanini, C.; Franko, M.Thermal Lens Spectrometric Determination of Colloidal and Ionic Silver in Water *Int. J. Thermophys.* 2011, 32, 818– 827, DOI: 10.1007/s10765-010-0856-z

[50]Tran, C. D.; Franko, M. Thermal Lens Spectroscopy. In *Encyclopedia of Analytical Chemistry*; Meyers, R. A., Ed.; John Wiley: Chichester, U.K., 2010; DOI: , DOI: 10.1002/9780470027318.a9079.

Supporting Information

One-Pot Synthesis of Biocompatible Silver Nanoparticle Composites from Cellulose and Keratin: Characterization and Antimicrobial Activity

ACS Applied materials & Interfaces, Vol 8, No. 50 (2016): pg. 34791-34801. DOI.

Supporting Information for

One-Pot Synthesis of Biocompatible Silver Nanoparticle Composites from Cellulose and Keratin: Characterization and Antimicrobial Activity

Chieu D. Tran[1]*, Franja Prosenc[2], Mladen Franko[2] and Gerald Benzi[1]

[1]Department of Chemistry, Marquette University,

P. O. Box 1881, Milwaukee, Wisconsin 53201-1881, USA

[2]Laboratory for Environmental Research, University of Nova Gorica,

Vipavska 13, 5000 Nova Gorica, Slovenia

*Corresponding Author: Tel: 1 414 288 5428; email: chieu.tran@marquette.edu

Measurements of Ag^0NPs released from [CEL+KER+ Ag^0NPs] Composites by Thermal Lens Method

Any possible AgNPs released from the composite materials was determined using the previously developed method. In this method, AgNPs were detected by measuring their surface plasmons resonance band at 409 nm by the thermal lens technique in a flow injection analysis (FIA). As described in the Experimental Section, AgNPs were produced by reducing Ag^+ with sodium borohydride, there is a remote possibility that some minute amount of Ag^+ may remained unreduced and remained in the composites (even though XRD results indicate that no Ag^+ is present in the composite) which was subsequently released. Because this thermal lens detection technique cannot detect any released Ag^+ as it does not have any surface plasmon resonance absorption, any released Ag^+ was converted into AgNPs by sodium borohydride directly by use of the FIA so that they can be readily detected. As a consequence, results obtained will provide information on two concentrations: colloidal silver concentration or (concentration of released AgNPs) and total silver concentration which is the sum of released AgNPs concentration plus released Ag^+ concentration.

The experimental setup to measure silver release was imitating the experimental setup used in bioassays.[SI-1] Composite materials of dimensions 3 x 20 mm^2 were put in sterile falcon tubes with 2 mL of sterile 1x PBS at pH 7.4. Three replicates each of blank samples ([CEL+KER]) and [CEL+KER + 500 mg Ag^0 NPs] composites were used. Tubes were put on a shaker at 400 rpm and kept at 37°C in darkness for 7 days. Samplings were conducted at time 0, 24 hrs, 3 days and 7 days. At every sampling 200 µL of sample was taken out of each tube and replaced with 200 µL of fresh PBS. The dilution was taken into account when calculating final concentrations. 100 µL of sample was reduced with 0.60 mM sodium borohydride ($NaBH_4$) in

order to measure total silver (AgNPs + Ag^{+}), whereas the other 100 µL of sample was not reduced in order to measure only colloidal silver (AgNPs) released from the sample. Sample preparation was done as shown on the Figure SI-1 below:

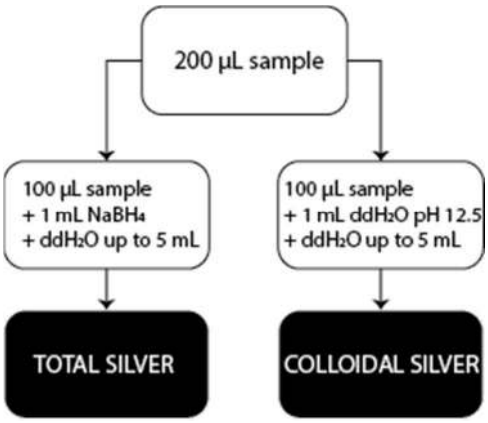

Figure S1: Sample preparation for silver release from the [CEL+KER+Ag^{0}NPs] composites.

Sample preparation was done in glass tubes wrapped in aluminum foil to protect it from light. Dilution made at sample preparation was taken into account when calculating measured concentrations.

All measurements were conducted on an in-house-built FIA system with a dual beam TLS detection unit.[S1,S2] The instrumental setup is schematically presented in Figure SI-2. Krypton laser operating at 407 nm (150 mW power) was used as a source of the pump-beam. The emission of a He-Ne laser (632.8 nm, 2 mW) served as a probe beam. The pump-beam modulation frequency was 40 Hz. Flow rate of the carrier (dd H_2O) was 0.600 mL/min. Sample was injected through the metal free injection valve, equipped with a 100 µL PEEK sample loop.

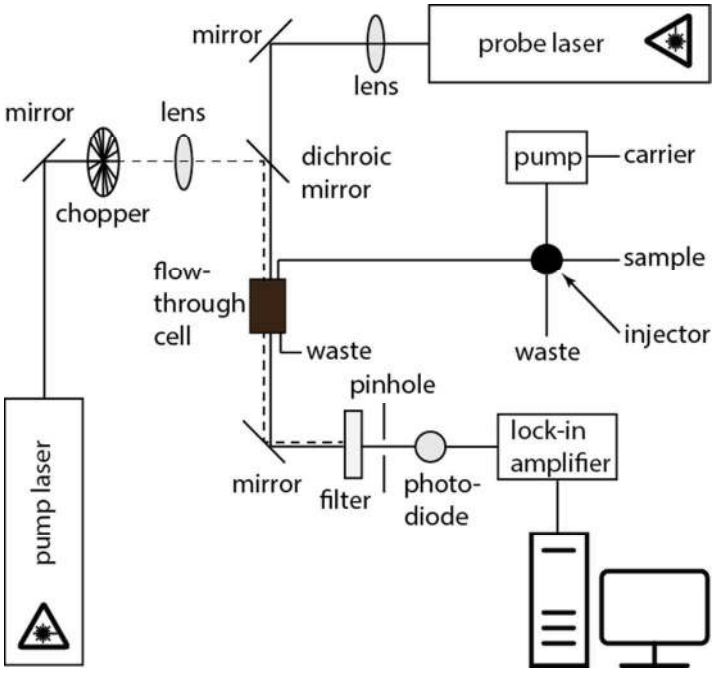

Figure S2: Schematic presentation of the FIA setup with thermal lens detection unit.

Separate calibration curve was prepared every time a set of samples was measured. Limit of detection (LOD) for this method was calculated as follows:

$$LOD = \frac{3 \cdot SD_{blank}}{k}$$

where SD_{blank} corresponds to standard deviation of blank signal, and k is the slope of the calibration curve.

To further confirm that the signals obtained are from the Ag^0NPs released from the [CEL+KER + Ag^0NPs] composites, additional experiment was designed in which nitric acid (HNO_3) was added to the released sample solution to dissolve the released Ag^0NPs. Specifically, 2.0 µL of concentrated HNO_3 was added to 6 mL of released sample to dissolve the Ag^0NPs. The Ag^+ obtained was then reconverted back to Ag^0NPs by addition of 6.0 mL PBS (pH 12.5) and 600 µL 0.6 mM $NaBH_4$ to 6 mL of dissolved sample. Samples at each stage of the

experiment (before dissolution, after dissolution, and after recovery) were measured on the FIA-thermal lens setup described above using the same conditions.

References

S1. Korte, D.; Bruzzoniti, M. C.; Sarzanini, C.; Franko, M. Thermal Lens Spectrometric Determination of Colloidal and Ionic Silver in Water. Int. J. Thermophys., **2011**, 32, 818-827.

S2. Tran, C. D.; Franko, M. Thermal Lens Spectroscopy" In: Encyclopedia of Analytical Chemistry, ed.: R.A. Meyers, John Wiley: Chichester., **2010**. DOI: 10.1002/9780470027318.a9079.